

# PCCP

Accepted Manuscript



This is an *Accepted Manuscript*, which has been through the Royal Society of Chemistry peer review process and has been accepted for publication.

*Accepted Manuscripts* are published online shortly after acceptance, before technical editing, formatting and proof reading. Using this free service, authors can make their results available to the community, in citable form, before we publish the edited article. We will replace this *Accepted Manuscript* with the edited and formatted *Advance Article* as soon as it is available.

You can find more information about *Accepted Manuscripts* in the [Information for Authors](#).

Please note that technical editing may introduce minor changes to the text and/or graphics, which may alter content. The journal's standard [Terms & Conditions](#) and the [Ethical guidelines](#) still apply. In no event shall the Royal Society of Chemistry be held responsible for any errors or omissions in this *Accepted Manuscript* or any consequences arising from the use of any information it contains.



PCCP

ARTICLE

## Difference in TiO<sub>2</sub> photocatalytic mechanism between rutile and anatase studied by detections of active oxygen and surface species in water

Yusuke Kakuma, Atsuko Y. Nosaka, and Yoshio Nosaka\*

Various kinds of TiO<sub>2</sub> photocatalysts have been widely applied for practical use. It is prerequisite to know the exact surface properties to develop further and efficient applications. However, the cause of the essential difference in the activities of two polymorphs of TiO<sub>2</sub>, rutile and anatase, was not clearly elucidated yet. We tried to clarify the cause in terms of active oxygen species ( $\bullet\text{OH}$ ,  $\bullet\text{O}_2^-$ , and H<sub>2</sub>O<sub>2</sub>) photogenerated on the surfaces, which are considered practically involved in the photocatalytic reactions. It was revealed that for anatase the rate of  $\bullet\text{OH}$  generation was high, but it decreased in the presence of H<sub>2</sub>O<sub>2</sub>. On the other hand, for rutile,  $\bullet\text{OH}$  generation was very small but it was increased with H<sub>2</sub>O<sub>2</sub>. The formation rate of  $\bullet\text{O}_2^-$  for rutile was higher than that for anatase, suggesting that the photoinduced reduction process should not be responsible for the higher photocatalytic activity of anatase. Since Ti-Ti distance of rutile surface could be smaller than that of anatase, rutile is capable of forming the surface structure such as Ti-OO-Ti, leading to form readily O<sub>2</sub>. The mechanism that the fast coupling of two photoinduced conduction band holes to form Ti-OO-Ti was proposed, which is responsible for the lower reactivity of rutile. This mechanism was verified by the analysis of surface species with ATR-IR spectroscopy.

Received 00th January 20xx,  
Accepted 00th January 20xx

DOI: 10.1039/x0xx00000x

[www.rsc.org/](http://www.rsc.org/)

### 1. Introduction

The photocatalytic reactions using light-irradiated semiconductor surface have been attracted much attention because they could be utilized for the conversion of solar energy to hydrogen fuels by light-induced water splitting.<sup>1,2</sup> Among the various semiconductor photocatalysts, titanium dioxide (TiO<sub>2</sub>) is a practical photocatalyst which can be applied to water purification and environmental cleaning owing to its high photocatalytic activity, chemical stability, no toxicity, and commercial availability.<sup>3-6</sup> Actually, TiO<sub>2</sub> photocatalysts have been utilized for self-cleaning tiles, glasses, and windows.<sup>7</sup> The details of the photocatalytic reactivity, however, is still under debate.<sup>8,9</sup> For example, the difference in the photocatalytic activities between two major polymorphs of TiO<sub>2</sub>, anatase and rutile, has not been clearly elucidated yet.<sup>8</sup> In general, anatase powders show significantly higher photocatalytic activity. On multivalent analyses for the correlation among structural and physical properties and photocatalytic activities for 35 differently prepared TiO<sub>2</sub> samples, it was clearly indicated that anatase is more active than rutile for the decomposition of organic compounds.<sup>10</sup> A lots of hypotheses have been proposed to explain the higher photocatalytic activity of anatase; i) higher potential of conduction band bottom for anatase crystal,<sup>11</sup> ii) higher mobility of carriers with a smaller

effective mass, iii) smaller crystallite size in general, iv) the longer lifetime of photoinduced  $e^- - h^+$  pairs originated from the nature of indirect band gap,<sup>12</sup> v) special surface active sites caused by the less dense crystal structure, and so on. However, for the oxygen evolution from water, rutile is reported to be superior to anatase.<sup>13</sup> The significant activity difference may depend on the properties of TiO<sub>2</sub> surface. The higher activity of anatase might be explained by the reduction ability of O<sub>2</sub> superior to rutile because of the higher conduction band level, and/or by a special surface interaction.

Active oxygen species ( $\bullet\text{OH}$ ,  $\bullet\text{O}_2^-$ , and H<sub>2</sub>O<sub>2</sub>) are the products generated on the TiO<sub>2</sub> surface by redox reactions of water and oxygen in the photocatalytic procedures. They are considered to be involved in the actual practical photocatalytic reactions. Previously, we revealed with a fluorescence probe method that  $\bullet\text{OH}$  radicals were formed from the trapped holes for anatase TiO<sub>2</sub>, while for rutile TiO<sub>2</sub> the Ti-peroxo (Ti-OO-Ti) site plays the role of a catalyst to generate OH radicals from water.<sup>14</sup> In the present study we investigated the difference of the surface oxidation processes for anatase and rutile in detail by use of chemiluminescence methods and proposed the most plausible reaction mechanisms, which were confirmed with the aid of the ATR-IR measurements.

### 2. Experimental Section

#### 2.1 Materials

Samples of anatase TiO<sub>2</sub> powder (ST-01, Ishihara Sangyo Ltd.) and rutile TiO<sub>2</sub> powder (MT-150A, TAYCA Ltd.) were used. Their

Department of Materials Science and Technology, Nagaoka University of Technology, Nagaoka, 940-2188 Japan  
\*E-mail : nosaka@nagaokaut.ac.jp

specific surface areas were 320 and 88 m<sup>2</sup>/g, respectively. The other properties of these TiO<sub>2</sub> powders have been described in the previous report.<sup>14</sup> The amount of the surface OH groups was checked by thermogravimetry with ThermoPlus EVO (TG8120, Rigaku, Inc.) as shown in Fig. 1. According to literature,<sup>15</sup> the physisorbed water which can be removed up to 150 °C had the densities of 5.4 and 5.0 molecules/nm<sup>2</sup> for anatase and rutile powders, respectively, while the densities of the chemisorbed OH group calculated from the weight loss between 150 and 600 °C were 4.9 and 12.9 molecules/nm<sup>2</sup> for anatase and rutile, respectively. In the calculation, the specific surface area stated above was used. For example, from the weight loss of anatase powder at 150 °C, the amount of physisorbed water was calculated as follows; 5.14 % × 6.02 × 10<sup>23</sup> molecules/mol / (18 g/mol × 320 m<sup>2</sup>/g) = 5.4 molecules/nm<sup>2</sup>. Thus rutile is covered with larger amount of chemisorbed water than anatase although the amount of physisorbed water was almost the same for two polymorphs.

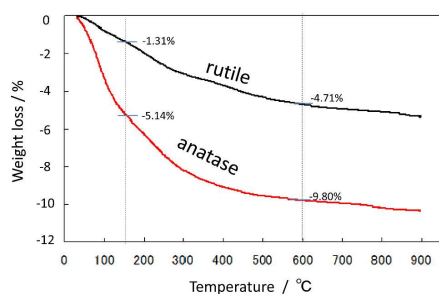


Fig. 1 Thermogravimetry of anatase and rutile powders used.

## 2.2 Detection of H<sub>2</sub>O<sub>2</sub>

The amount of H<sub>2</sub>O<sub>2</sub> was evaluated by a lucigenin chemiluminescence method.<sup>16</sup> Fifteen mg of TiO<sub>2</sub> powder was suspended in 3.5 mL of purified water in a quartz cell (1 cm × 1 cm × 4.5 cm) and stirred with a magnetic stirrer in a dark box. The pH of the suspension was adjusted to 9 with NaOH.<sup>17</sup> The cell containing the suspension was irradiated with UV light using an LED source (5 mW/cm<sup>2</sup> at 365 nm, LC-L201, Hamamatsu Photonics). After the UV irradiation, 50 μL of 0.7 mM lucigenin solution was added with a micro-syringe to observe the chemiluminescence. The chemiluminescence light was guided to the photomultiplier (R2693P, Hamamatsu) through a UV sharp cut filter. The signal of the photomultiplier was introduced into photon counting unit (C3866 and C8855, Hamamatsu) to be recorded by a desktop computer. The number of photons recorded as a function of time up to 100 s was integrated to evaluate the H<sub>2</sub>O<sub>2</sub> concentration. The concentration of H<sub>2</sub>O<sub>2</sub> was calibrated by measuring the chemiluminescence intensity for the known concentration of H<sub>2</sub>O<sub>2</sub> solution in the absence of TiO<sub>2</sub> powders. Therefore, the calculated concentration for the suspension may have some errors caused by the scattering of the chemiluminescence.

H<sub>2</sub>O<sub>2</sub> adsorption property of TiO<sub>2</sub> was evaluated in dark by measuring the concentration of H<sub>2</sub>O<sub>2</sub> in the solution. The lucigenin chemiluminescence method was also employed to evaluate the concentration of 0.3-mM H<sub>2</sub>O<sub>2</sub> solutions after the addition of TiO<sub>2</sub> powders. The decrease of the H<sub>2</sub>O<sub>2</sub> concentration in solution provided the amount of adsorbed H<sub>2</sub>O<sub>2</sub> and the intrinsic adsorbed

molecules were calculated with the BET surface area of the TiO<sub>2</sub> powders.

## 2.3 Detection of superoxide radicals (•O<sub>2</sub><sup>-</sup>)

The amount of photocatalytically generated •O<sub>2</sub><sup>-</sup> was measured by the chemiluminescence method with MCLA (Methoxy Cypridina Luciferin Analog, 2-methyl-6-(p-methoxyphenyl)-3,7-dihydroimidazo(1,2-a)pyrazin-3-one hydrochloride, Tokyo Chemical Industry). The experimental procedure was the same as that for the H<sub>2</sub>O<sub>2</sub> detection described above, except that the solution pH was not adjusted to be 5.2. After the UV irradiation, 50 μL of 0.35-mM MCLA aqueous solution was added to the cell, and then the intensity of chemiluminescence caused by •O<sub>2</sub><sup>-</sup> was detected with the photon counting system described above. Integration of the intensity was proportional to the •O<sub>2</sub><sup>-</sup> concentration. To calibrate the MCLA chemiluminescence intensity, a luminol chemiluminescence method,<sup>18</sup> by which •O<sub>2</sub><sup>-</sup> concentration can be quantitated, was employed for a standard suspension of alkaline solution.

## 2.4 Detection of •OH radicals

The amount of •OH produced in photocatalysis was measured by a coumarin fluorescence probe method.<sup>19</sup> The same cell and UV source mentioned above were used for this measurement. Fifteen mg of TiO<sub>2</sub> was suspended in 3.5 mL of 0.1-mM coumarin aqueous solution. After UV irradiation, 0.5 g of KCl was added to the suspension to precipitate TiO<sub>2</sub> powders from the suspension and then it was stored in dark for one day. After that, the fluorescence spectrum of the supernatant solution was measured with a fluorescence spectrophotometer (Model 850, Hitachi). Since 6.1% of •OH can be converted to umbelliferone in 0.1-mM coumarin aqueous solution,<sup>14</sup> the •OH concentration could be calculated by use of this conversion factor. It should be noted that, since the probe molecules are present in solution during the irradiation, the obtained •OH concentration is that accumulated during the irradiation. Therefore, the time profile of •OH is different from those of H<sub>2</sub>O<sub>2</sub> and •O<sub>2</sub><sup>-</sup>, in which the probe molecules were added after stopping the irradiation.

To examine the effect of H<sub>2</sub>O<sub>2</sub> as the reaction intermediate, H<sub>2</sub>O<sub>2</sub> of up to 0.8 mM was added in the reaction solution before the UV irradiation. The amounts of •O<sub>2</sub><sup>-</sup> and •OH after the 60-s irradiation were measured by varying the concentration of added H<sub>2</sub>O<sub>2</sub>.

## 2.5 ATR-IR measurements

The chemical structure of TiO<sub>2</sub> surface was examined with attenuated total reflectance infrared (ATR-IR) measurements. FT-IR spectrometer used was an FTS-7000e (Varian, Agilent) with an mercury cadmium telluride (MCT) detector and a Ge/KBr beam splitter which was operated at resolution of 4 cm<sup>-1</sup> with an accumulation of 128 times. A diamond ATR (MIRacle P025-9010, PKE Technologies) for single diffraction was employed to measure the surface of TiO<sub>2</sub> powder in solution. To photo irradiate TiO<sub>2</sub>, a 20 mW diode laser of 376 nm (TC20-0375, NeoArk) was used.

The TiO<sub>2</sub> sample for ATR-IR measurements was prepared as follows. 120 mg of TiO<sub>2</sub> powders were dispersed in 10 mL of water with ultrasonic agitation, then 30 μL of the suspension was placed on the surface of the diamond prism of ATR and dried under ambient atmosphere in dark for a night. After adding 150 μL of pure

water, the measurements of IR spectra were started using the stored spectrum of water as a reference. In some cases, D<sub>2</sub>O was used in place of water. Since H atom of the surface species is replaced with D in D<sub>2</sub>O, the peak position largely shifts when the vibrational mode is assigned to the group containing H atom. An O-ring and cover-glass was used to prevent the evaporation of the solution. After an equilibrium surface state was reached in 60 min, UV light of the 376 nm laser was irradiated during the measurements. For the addition of H<sub>2</sub>O<sub>2</sub>, a half of the solution was replaced with an appropriate concentration of H<sub>2</sub>O<sub>2</sub> solution not to disturb the particle arrangements. The thicknesses of the TiO<sub>2</sub> layer were calculated to be 73 and 66 μm for anatase and rutile powders, respectively, by assuming the fill factor of 50% and the sphere of the primary particle. Since the penetration depth of the ATR is calculated to be 0.5–3.0 μm at 4000–500 cm<sup>-1</sup>, IR spectra reflect mainly the surface of the TiO<sub>2</sub> powders located near the bottom of the layer. Since the UV laser irradiated the TiO<sub>2</sub> layer from the top, the excitation efficiency at the observed TiO<sub>2</sub> particles was not so high, as compared to the aqueous suspension.

### 3. Results and Discussion

#### 3.1 Generation of active oxygens

At first, the generation of H<sub>2</sub>O<sub>2</sub>, which is the only stable species among the active oxygen species, was examined by the lucigenin chemiluminescence method. After stopping the UV irradiation, chemiluminescence was observed on the addition of lucigenin. The luminescence intensity decayed with time owing to the consumption of the generated H<sub>2</sub>O<sub>2</sub> (see Fig. 2A). From the integrated luminescence intensity, the concentration of H<sub>2</sub>O<sub>2</sub> produced by the irradiation was calculated.

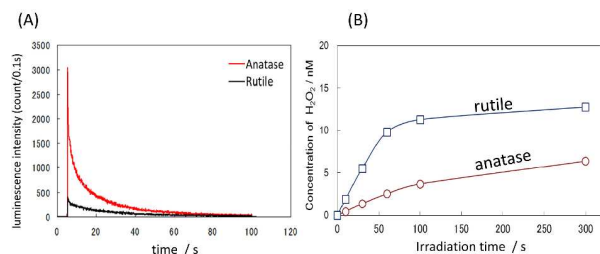
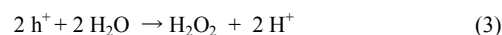


Fig. 2 (A) Time profile of the chemiluminescence on the addition of lucigenin after 60 s UV irradiation. (B) H<sub>2</sub>O<sub>2</sub> concentration evaluated from the chemiluminescence intensity as a function of the UV irradiation time for aqueous suspension of anatase (○) and rutile (□) TiO<sub>2</sub> nano-particles.

Figure 2B shows the generation of H<sub>2</sub>O<sub>2</sub> under UV irradiation on powder suspensions of anatase and rutile TiO<sub>2</sub>. The generation rate of H<sub>2</sub>O<sub>2</sub> for rutile was 2–3 times larger than that for anatase. The surface area of anatase is larger by 3.6 times than that of rutile and the excitation rate of 365 nm light for rutile was almost the same as that for anatase.<sup>20</sup> Therefore, the surface area and excitation rate would not be responsible for the larger production of H<sub>2</sub>O<sub>2</sub> for rutile in Fig. 2. The problem is that the adsorbed H<sub>2</sub>O<sub>2</sub> cannot be detected actually by the chemiluminescence method. Hence next the adsorption of H<sub>2</sub>O<sub>2</sub> was measured. The specific adsorptions of H<sub>2</sub>O<sub>2</sub>

for anatase and rutile particles were obtained to be 0.06 and 0.26 molecules/nm<sup>2</sup>, respectively. Thus taking account of the larger adsorption of H<sub>2</sub>O<sub>2</sub> for rutile, the experimental result of Fig. 2 indicates that the formation of H<sub>2</sub>O<sub>2</sub> is significantly larger for rutile.

The photocatalytic generation of H<sub>2</sub>O<sub>2</sub> could be expressed by the following equations. The photoexcitation of TiO<sub>2</sub> causes electrons (e<sup>-</sup>) and holes (h<sup>+</sup>) at the conduction band and valence band, respectively, eqn (1). Then, H<sub>2</sub>O<sub>2</sub> was produced by the reduction of O<sub>2</sub> in air with e<sup>-</sup>, eqn (2), and the oxidation of water takes place with h<sup>+</sup>, eqn (3).



To clarify the detail of the two-electron reactions, eqn (2) and eqn (3), the one-electron reduction step, eqn (4), and one-electron oxidation step, eqn (5), were also examined by the measurements of the products, •O<sub>2</sub><sup>-</sup> and •OH, respectively.

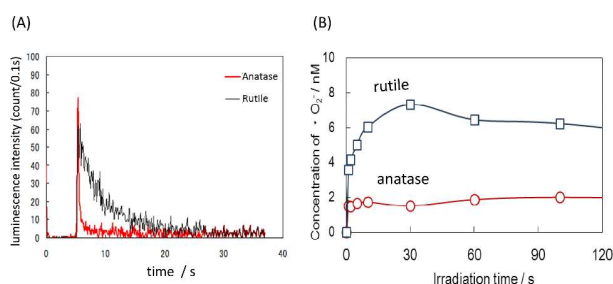
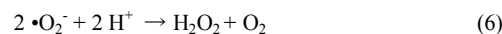
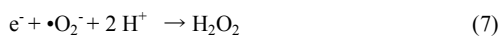


Fig. 3 (A) Chemiluminescence intensity of MCLA observed after 60 s UV irradiation. (B) •O<sub>2</sub><sup>-</sup> generation measured from MCLA chemiluminescence as a function of the time of UV irradiation on aqueous suspension of anatase (○) and rutile (□) TiO<sub>2</sub> nano-particles.

At first, the one-electron reduction of O<sub>2</sub> was examined by measuring the generation of •O<sub>2</sub><sup>-</sup> by means of the chemiluminescence method with MCLA after stopping the UV irradiation. The intensity decayed after the addition of MCLA due to the consumption of •O<sub>2</sub><sup>-</sup> (Fig. 3A). The integrated chemiluminescence intensity reflects the concentration of •O<sub>2</sub><sup>-</sup> produced by the irradiation. The amount of •O<sub>2</sub><sup>-</sup> produced by the UV irradiation was plotted in Fig. 3B as a function of the UV irradiation time. As shown in Fig. 3B, rutile TiO<sub>2</sub> generated a larger amount of •O<sub>2</sub><sup>-</sup> than anatase. The production of •O<sub>2</sub><sup>-</sup> was increased initially in a short period and reached to a steady state, indicating that a further reaction to form H<sub>2</sub>O<sub>2</sub> by disproportionation<sup>21</sup>, eqn (6), and/or further reduction, eqn (7), to form H<sub>2</sub>O<sub>2</sub> proceeded.





The larger amount of  $\bullet\text{O}_2^-$  detected for rutile indicates that rutile produces  $\bullet\text{O}_2^-$  more preferably than anatase. This observation is consistent with the previous report in which the generation of  $\bullet\text{O}_2^-$  was measured by luminol chemiluminescence in alkaline solution for several kinds of  $\text{TiO}_2$  powders.<sup>22</sup> When the production of  $\text{H}_2\text{O}_2$  (Fig. 2B) was compared with that of  $\bullet\text{O}_2^-$  (Fig. 3B), rutile is found to be more preferable for the both productions, namely  $\bullet\text{O}_2^-$  and  $\text{H}_2\text{O}_2$ . Taking account that the photocatalytic oxidation should take place simultaneously with the reduction, one could conclude that the oxidation ability of rutile for  $\text{H}_2\text{O}$  is significantly larger than that of anatase.

To clarify the oxidation process of  $\text{H}_2\text{O}$ , the formation of another one-electron-oxidation product,  $\bullet\text{OH}$ , was measured by a coumarin fluorescence probe method. On the photoirradiation of anatase and rutile powder suspensions in the presence of coumarin, a new fluorescence band attributable to the  $\bullet\text{OH}$  adduct of coumarin, umbelliferone, was observed for anatase (Fig. 4A) but not for rutile. From the fluorescence intensity, the concentration of  $\bullet\text{OH}$  was calculated and plotted in Fig. 4B as a function of the irradiation time. As shown in Fig. 4B, for anatase  $\text{TiO}_2$  the production of  $\bullet\text{OH}$  was increased almost proportionally to the irradiation time. On the other hand, for rutile  $\text{TiO}_2$  the  $\bullet\text{OH}$  formation was scarcely observed, though the slight amount of  $\bullet\text{OH}$  was detected after 100 s irradiation. The higher generation of  $\bullet\text{OH}$  for anatase agrees well with the previous report,<sup>20</sup> in which the decomposition rate of alcohols was parallel to the  $\bullet\text{OH}$  formation rate. The lack of  $\bullet\text{OH}$  generation by reaction (5), responsible for the small generation of  $\bullet\text{OH}$ , may suggest that the direct two-electron oxidation, eqn (3), of water should be dominant to form  $\text{H}_2\text{O}_2$  for rutile since the formation of  $\text{H}_2\text{O}_2$  is larger for rutile as described above.

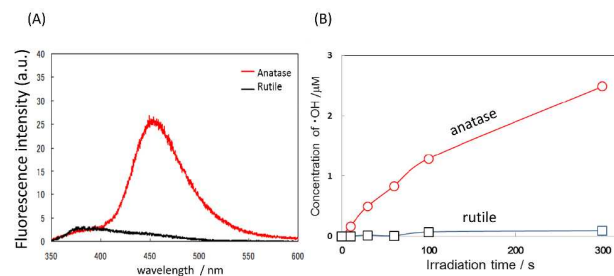


Fig. 4 (A) Fluorescence spectra measured after 300 s UV irradiation for anatase and rutile  $\text{TiO}_2$  suspension containing 0.1 mM coumarin. (B) OH radical generation calculated from fluorescence intensity as a function of the UV irradiation time for aqueous suspension of anatase (o) and rutile (□)  $\text{TiO}_2$  nano-particles.

To clarify the processes of the active oxygen formation, the effects of the addition of  $\text{H}_2\text{O}_2$  on the formation of  $\bullet\text{O}_2^-$  and  $\bullet\text{OH}$  were examined. As shown in Fig. 5A, the  $\bullet\text{O}_2^-$  formation increased with  $\text{H}_2\text{O}_2$  significantly for anatase  $\text{TiO}_2$ , suggesting the oxidation of  $\text{H}_2\text{O}_2$  by valence band holes, eqn (8), with the acceleration of the reduction of  $\text{O}_2$  to produce  $\bullet\text{O}_2^-$ , eqn (4).

For rutile, the increase of  $\bullet\text{O}_2^-$  was less than anatase  $\text{TiO}_2$ . The smaller increase suggests that the oxidation of  $\text{H}_2\text{O}_2$  should accelerated the reduction of  $\text{O}_2$  to generate  $\bullet\text{O}_2^-$ , eqn (4), but that the oxidation of  $\text{H}_2\text{O}_2$ , eqn (8) might not contribute to the  $\bullet\text{O}_2^-$  generation. Because the  $\text{O}_2$  production for rutile is more preferable than that for anatase,<sup>13</sup>  $\text{H}_2\text{O}_2$  may be oxidized by two holes to form  $\text{O}_2$ , eqn (9).

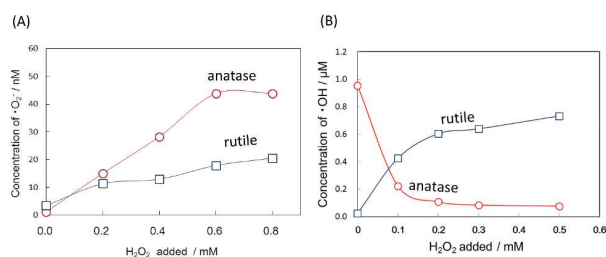
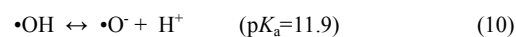


Fig. 5 Effect of  $\text{H}_2\text{O}_2$  on the (A)  $\bullet\text{O}_2^-$  and (B)  $\bullet\text{OH}$  generations measured after the 60-s UV irradiation on aqueous suspension of anatase (o) and rutile (□)  $\text{TiO}_2$  nano-particles.

The effect of  $\text{H}_2\text{O}_2$  addition on the  $\bullet\text{OH}$  generation was examined and plotted in Fig. 5B. For anatase  $\bullet\text{OH}$  formation decreased with the additional  $\text{H}_2\text{O}_2$ , while it increased for rutile. This notable observation was found previously by using several fluorescence probes, such as terephthalic acid,<sup>22</sup> coumarin,<sup>14</sup> and 3-carboxy coumarin.<sup>14</sup> The decrease of  $\bullet\text{OH}$  formation for anatase in Fig. 5B may be explained by that the oxidation of  $\text{H}_2\text{O}$ , eqn (5), was replaced by the oxidation of  $\text{H}_2\text{O}_2$ , eqn (8), because the oxidation potential of  $\text{H}_2\text{O}_2$  ( $E^0 = 1.48 \text{ V}$  vs. SHE at pH=0) is smaller than that of  $\text{H}_2\text{O}$  ( $E^0 = 2.7 \text{ V}$ ).<sup>23</sup> The increase of  $\bullet\text{OH}$  for rutile might be explained by the reduction of  $\text{H}_2\text{O}_2$  as was suggested previously.<sup>22</sup> However, since the reduction of  $\text{O}_2$ , eqn (4), was not decreased with  $\text{H}_2\text{O}_2$  as shown in Fig. 5A, the formation of  $\bullet\text{OH}$  should be attributed to the oxidation of  $\text{H}_2\text{O}$ , eqn (5), assisted by the presence of  $\text{H}_2\text{O}_2$ . In our recent study on the oxidation process at single crystalline rutile photoelectrodes, the formation of OH radicals as a by-product of  $\text{O}_2$  formation was suggested.<sup>24</sup> That is, adsorbed  $\text{H}_2\text{O}_2$ , which is the intermediate in the  $\text{O}_2$  production at rutile  $\text{TiO}_2$  surface, acts as a catalyst to produce OH radicals.

Thus, the plausible mechanisms of the photocatalytic  $\bullet\text{OH}$  formation procedure for anatase and rutile could be illustrated individually in Fig. 6. For anatase, photoinduced valence band holes are trapped at bridged OH sites of  $\text{TiO}_2$  surface to become trapped holes. Electron spin resonance (ESR) studies showed that the structure of the trapped holes for anatase was not the same as that of the adsorbed  $\bullet\text{OH}$  species.<sup>25</sup> However,  $\bullet\text{OH}$  can be in the equilibrium with  $\bullet\text{O}^-$ , eqn (10),<sup>23</sup> where  $\text{p}K_a$  may vary with the adsorption.<sup>19</sup>



Therefore, the trapped holes cannot be distinguished from the adsorbed OH radicals. The ratio of OH radicals in solution to the surface holes was estimated to be about 0.01.<sup>20</sup>

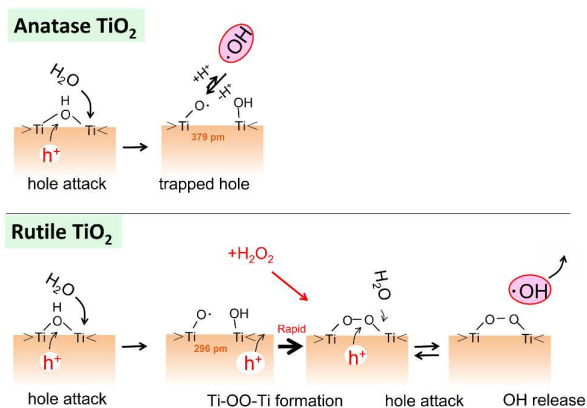


Fig. 6 Plausible mechanisms of  $\bullet\text{OH}$  generation at the surface of anatase and rutile  $\text{TiO}_2$  to explain the observations for Fig. 5B

On the other hand, for rutile, the photoinduced valence band hole is rapidly trapped at oxygen adjacent to the hole to form  $\text{Ti-OO-Ti}$  structure at the surface.<sup>26</sup> Since it is equivalent to the adsorbed  $\text{H}_2\text{O}_2$ , a small fraction of  $\bullet\text{OH}$  could be produced at the rutile surface by the oxidation of  $\text{H}_2\text{O}$  owing to the  $\text{Ti-OO-Ti}$  structure.<sup>24</sup>

The difference in the formation process of  $\bullet\text{OH}$  radicals between anatase and rutile could be explained by the  $\text{Ti-Ti}$  distance of two  $\text{Ti}$  atoms forming a bridged  $\text{OH}$  site. According to the study of the  $\text{PbO}_2$  deposition on  $\text{TiO}_2$ , an oxidation site of  $\text{TiO}_2$  locates on the surface of anatase (001) and rutile (011).<sup>27</sup> Based on the crystalline structure, the  $\text{Ti-Ti}$  distances are 379 and 296 pm for anatase and rutile, respectively. Thus, the holes trapped at the bridged  $\text{O}$  site are rather distant each other at the anatase surface, while at the rutile surface they locate short enough capable to form a couple. This concept would be supported by the fact that the specific adsorption of  $\text{H}_2\text{O}_2$  is significantly larger for rutile than anatase as stated above.

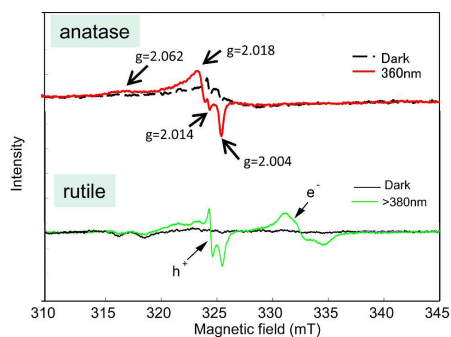


Fig. 7 ESR spectra of anatase and rutile  $\text{TiO}_2$  powders measured at 77 K as the effect of UV irradiation, taken from the references 28 (©Springer, 2012) and 29 (© Elsevier, 2014).

Figure 7 shows ESR spectra of anatase and rutile  $\text{TiO}_2$  powders measured at 77K as the effect of UV light irradiation, which

have been reported previously.<sup>28,29</sup> For anatase, signals similar to the photoinduced-trapped holes appeared before photo irradiation, and the trapped electron disappeared due to the recombination with the trapped holes after the photoirradiation, indicating the presence of relatively-stable trapped holes. On the other hand, for rutile powder, the signal of the trapped holes was relatively small and the signal of the trapped electrons appeared. This observation is consistent with the proposed surface reaction by which at the rutile surface the trapped holes are diminished by coupling.

### 3.2 Change of $\text{TiO}_2$ surfaces on the irradiation

The difference in the surface process for anatase and rutile  $\text{TiO}_2$  stated above was analysed for the interface of the photocatalyst and water by ATR-IR spectroscopy. For the proper comparison with the above experimental results, the samples were prepared without any pre-treatment and measured under the same condition, namely, in the presence of  $\text{O}_2$  without the addition of any electron acceptor.

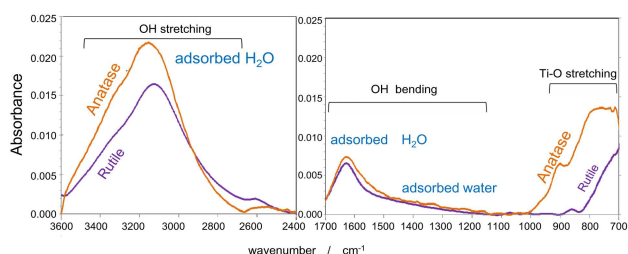


Fig. 8 ATR-IR absorption spectra of anatase and rutile  $\text{TiO}_2$  nano-powders spread over the ATR prism surface. The reference was bulk water without  $\text{TiO}_2$  powders.

Figure 8 shows the ATR-IR spectra for anatase and rutile  $\text{TiO}_2$  powders. Since the diamond used as the ATR prism shows absorption from 2300 to 1800  $\text{cm}^{-1}$ , the middle part of the spectra was excluded. Signals observed ranging from 3600 to 2600  $\text{cm}^{-1}$  are attributable to the stretching mode of  $\text{OH}$  group under some environments.<sup>30</sup> The  $\text{HOH}$  bending mode corresponding to the stretching mode was observed as a peak at 1620  $\text{cm}^{-1}$ .<sup>31</sup> The absorption of the  $\text{OH}$  bending mode is expanded down to 900  $\text{cm}^{-1}$ . Strong absorption due to  $\text{Ti-O}$  stretching mode<sup>32</sup> was observed in the wave number region smaller than 1000  $\text{cm}^{-1}$  for anatase and 900  $\text{cm}^{-1}$  for rutile crystallites.

Figure 9A shows the change of the ATR-IR spectra with the UV irradiation for anatase and rutile powder layers. A broad peak at 3200  $\text{cm}^{-1}$  is attributable to  $\text{O-H}$  stretching mode associated with bridged  $\text{OH}$  ( $\text{b-OH}$ ) groups.<sup>30</sup> For rutile this signal was decreased rapidly (within 5 min) by UV irradiation, indicating the release of  $\text{b-OH}$  by trapping of holes as suggested by Nakamura et al.<sup>26</sup> and Salvador.<sup>9</sup> The peak at 1332  $\text{cm}^{-1}$  increased along with the increase of the peaks at 1569 and 1593  $\text{cm}^{-1}$ , which could be observed even in  $\text{D}_2\text{O}$  (Fig. 9B). These peaks could be assigned to the  $\text{CO}$  stretching mode of  $\text{HCO}_3^-$ .<sup>33</sup> Since  $\text{CO}_2$  in air was dissolved in solution as a form of  $\text{HCO}_3^-$ , it photoadsorbed on the surface of  $\text{TiO}_2$ . The broad signal ranging from 1100 to 900  $\text{cm}^{-1}$  could be attributed to  $\text{Ti-OO}^-$  based on the spectral change with  $\text{H}_2\text{O}_2$  in the following experiments and the spectra in  $\text{D}_2\text{O}$  (Fig. 9B). Since oxygen was not removed in the present study, photoadsorbed  $\bullet\text{O}_2^-$  may cause the change in the IR spectra of this broad signal region. It is notable that for rutile the

absorption peak at about  $930\text{ cm}^{-1}$  was observed under UV irradiation, which may be assigned to Ti-OO-Ti from the following experiments

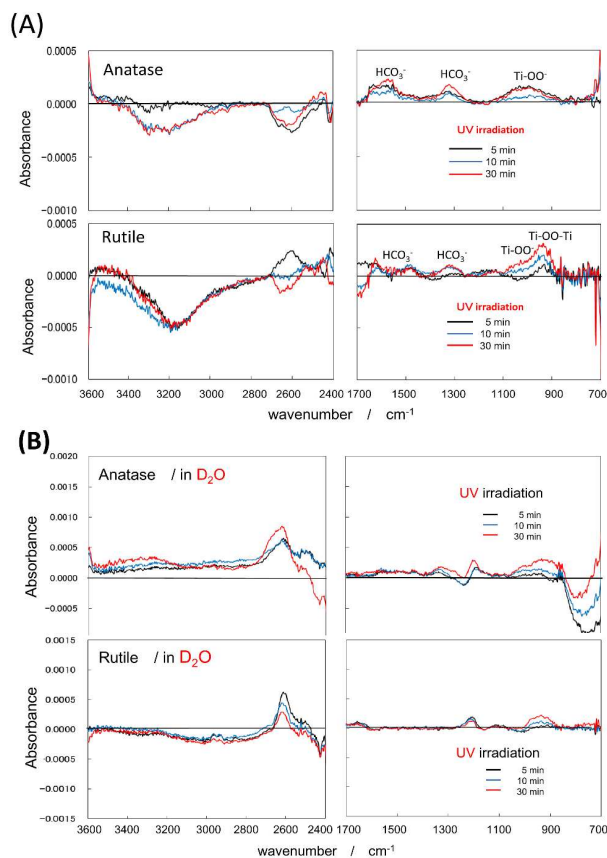


Fig. 9 Change of the ATR-IR spectra of anatase and rutile  $\text{TiO}_2$  nano-powder films in (A)  $\text{H}_2\text{O}$  and (B)  $\text{D}_2\text{O}$  with the UV irradiation for 5, 10, and 30 min.

Figure 10A shows the effect of adsorption of the addition of  $\text{H}_2\text{O}_2$  on the anatase and the rutile surface. The IR spectrum of  $0.5\text{ mM H}_2\text{O}_2$  in water is negligibly small as shown in Fig. 10B. In this figure, the spectra of  $\text{H}_2\text{O}_2$  of different concentrations down to  $10\text{ mM}$  were shown and a peak of O-O stretching mode was observed at  $900\text{ cm}^{-1}$ . Since the IR spectra of aqueous solution of  $0.5\text{ mM H}_2\text{O}_2$  could not be observed, the difference in the IR spectra with  $0.5\text{ mM H}_2\text{O}_2$  (Fig. 10A) would be caused by the adsorption of  $\text{H}_2\text{O}_2$  on  $\text{TiO}_2$  surface.

For rutile, the decrease of the broad absorption band  $1200 - 900\text{ cm}^{-1}$  in Fig. 10A could be attributed to the release of adsorbed water, and the sharp increase of absorption band at  $934\text{ cm}^{-1}$  could be attributed to the adsorbed  $\text{H}_2\text{O}_2$  species. For anatase, terminal water at around  $3300\text{ cm}^{-1}$ , which is associated with OH stretching of terminal OH sites,<sup>30</sup> decreased with the adsorption of  $\text{H}_2\text{O}_2$ . And the increase of adsorbed water at  $1150-900\text{ cm}^{-1}$  could be attributed to the adsorption of  $\text{H}_2\text{O}_2$  in a form different from rutile, probably as a form of  $-\text{OO}-$ .

Thus, the distinct signal at  $934\text{ cm}^{-1}$  was observed only for rutile on irradiation (Fig. 9A) and by adsorption of  $\text{H}_2\text{O}_2$  (Fig. 10A).

Therefore, ATR-IR observation clearly showed that on the UV irradiation the surface structure of rutile changes to that covered with the adsorbed  $\text{H}_2\text{O}_2$  as suggested by the analysis of active oxygens stated above. Consequently, the surface structure of rutile was found to be considerably different from that of anatase.

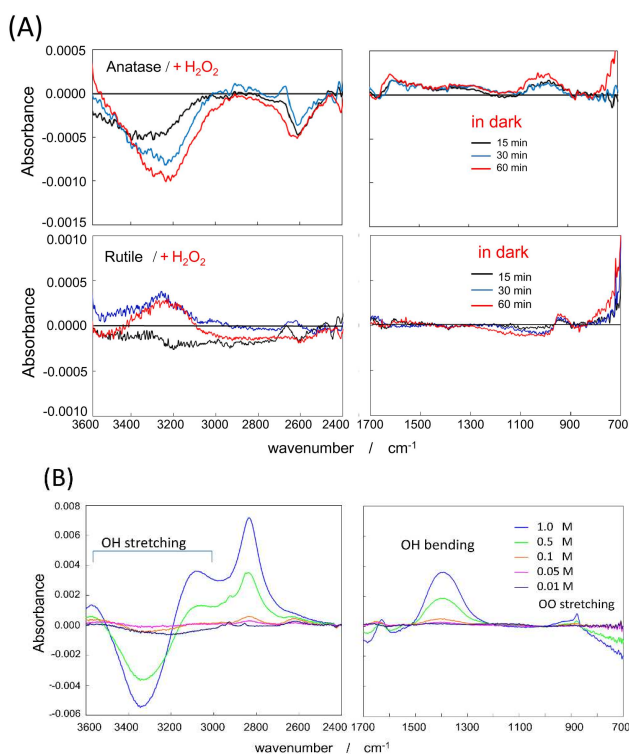


Fig. 10 (A) Change of the ATR-IR spectra of anatase and rutile  $\text{TiO}_2$  nano-powder films in  $\text{H}_2\text{O}$  at 15, 30, and 60 min after the addition of  $0.5\text{ mM H}_2\text{O}_2$ . (B) ATR-IR spectra of 1.0, 0.5, 0.1, 0.05, 0.01 M  $\text{H}_2\text{O}_2$  aqueous solution relative to that of pure water.

### 3.3 Oxidation mechanisms on anatase and rutile $\text{TiO}_2$

Based on the above mentioned results on the photocatalytic oxidation processes at the anatase and rutile  $\text{TiO}_2$  surfaces, the most plausible processes could be summarized as is illustrated in Fig. 11.

The lifetime of trapped holes was suggested to be longer than  $1\text{ s}$  for anatase  $\text{TiO}_2$ .<sup>34</sup> Furthermore, it was revealed that the photocatalytic activity of the oxidation of organic compounds (RH) was related to the produced amount of  $\bullet\text{OH}$  but the oxidation was mainly caused by the surface trapped holes, which was verified through the quantitative analysis of  $\bullet\text{OH}$ .<sup>20</sup> Taking account of these facts, the oxidation at the anatase surface must proceed as is illustrated in Fig. 11.

It is notable as stated above that for rutile surface the distance between two adjacent surface Ti atoms is  $296\text{ pm}$ , while it is  $379\text{ pm}$  for anatase. Since the actual O-O bond length is  $146\text{ pm}$ , and the Ti-O-O angle should be near  $90^\circ$ , it would be difficult to form Ti-OO-Ti structure at the anatase surface. This difficulty would be responsible for the relatively longer lifetime of the surface trapped holes for anatase  $\text{TiO}_2$ .

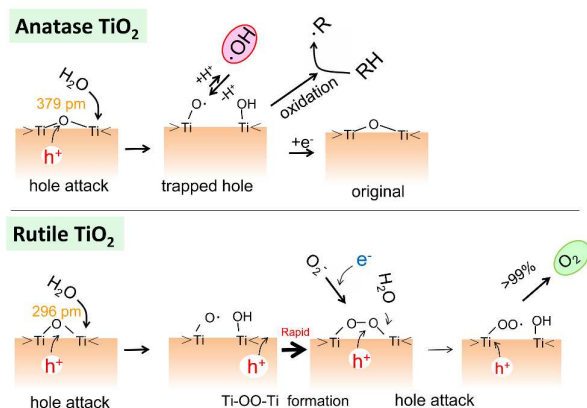


Fig. 11 Plausible photocatalytic actions at the surface of  $\text{TiO}_2$ . The oxidation of organic molecule for anatase, and that of water for rutile polymorphs.

For rutile, due to the shorter separation distance between Ti at the surface, the trapped holes could easily form a dimer to generate a Ti-OO-Ti structure, which is not active for the oxidation of organic compounds. Thus, the formation of a trapped-hole dimer would be responsible for the low activity of rutile  $\text{TiO}_2$  for the oxidation of organic compounds. On the other hand, the formation of Ti-OO-Ti structure is essential to produce  $\text{O}_2$  by four electron oxidation of water. Thus, the larger activity of rutile for  $\text{O}_2$  production could be explained.

#### 4. Conclusions

$\text{TiO}_2$  photocatalysts have been practically applied in various fields. The two polymorphs of  $\text{TiO}_2$ , rutile and anatase, are known to present different physical properties and show different photocatalytic activities. However, the cause has not been clearly elucidated yet. If we can clarify the cause the more efficient and diverse applications could be developed. In this study we tried to clarify the cause in terms of active oxygen species ( $\bullet\text{OH}$ ,  $\bullet\text{O}_2^-$ , and  $\text{H}_2\text{O}_2$ ) photogenerated on the surfaces, which are considered practically involved in the photocatalytic reactions.

It was revealed that the formation of  $\text{H}_2\text{O}_2$  for rutile was significantly higher than that for anatase but  $\bullet\text{OH}$  generation was very small. On the other hand, the formation rate of  $\bullet\text{O}_2^-$  for rutile was higher than that for anatase, suggesting that the higher activity of anatase should not be attributed to the photoinduced reduction process.

Since Ti-Ti distance of rutile surface could be smaller than that of anatase, rutile is capable of forming the surface structure such as Ti-OO-Ti, which corresponds to the adsorbed  $\text{H}_2\text{O}_2$ , leading to form readily  $\text{O}_2$  by further oxidation. The mechanism that the fast coupling of two photoinduced conduction band holes to form Ti-OO-Ti was proposed as the cause of the lower photocatalytic reactivity of rutile, which was verified by the analysis of the photogenerated surface species on  $\text{TiO}_2$  with ATR-IR spectroscopy.

#### Acknowledgement

We thank Mr. Kazuya Ota of Asahi Kasei Chemicals Co. for his support to the research.

#### References

- 1 A. Fujishima, K. Honda, *Nature* **1972**, *238*, 37–38.
- 2 A. Kudo, Y. Miseki, *Chem. Soc. Rev.* **2009**, *38*, 253–278.
- 3 *Photocatalysis: Science and Technology*, (Eds.: M. Kaneko, I. Ohkura), Kodansha-Springer, Tokyo, **2002**.
- 4 K. Hashimoto, H. Irie, A. Fujishima, *TiO<sub>2</sub> Photocatalysis: A Historical Overview and Future Prospects*, *Jpn. J. Appl. Phys.* **2005**, *44*, 8269–8285.
- 5 *Environmentally Benign Photocatalysts; Applications of Titanium Oxide-based Materials*, (Eds.: M. Anpo, P. V. Kamat), Springer, New York, **2010**.
- 6 *Photocatalysis and Water Purification*, (Eds. P. Pichat), Wiley-VCH: Weinheim, Germany, **2013**.
- 7 A. Fujishima, X. Zhang, D. Tryk, *Surf. Sci. Rep.* **2008**, *63*, 515–582.
- 8 M. A. A. Henderson, *Surf. Sci. Rep.* **2011**, *66*, 185–297.
- 9 P. Salvador, *Prog. Surf. Sci.* **2011**, *86*, 41–58.
- 10 O. O. Prieto-Mahaney, N. Murakami, R. Abe, B. Ohtani, *Chem. Lett.* **2009**, *38*, 238–239.
- 11 L. Kavan, M. Graetzel, S. E. Gilbert, C. Klemenz, H. J. Scheel, *J. Am. Chem. Soc.* **1996**, *118*, 6716–6723.
- 12 M. Xu, Y. Gao, E. M. Moreno, M. Kunst, M. Muhler, Y. Wang, H. Idriss, C. Woll, *Phys. Rev. Lett.* **2011**, *106*, 138302.
- 13 B. Ohtani, O. O. Prieto-Mahaney, D. Li, R. Abe, *J. Photochem. Photobiol. A*, **2010**, *216*, 179–182.
- 14 J. Zhang, Y. Nosaka, *J. Phys. Chem. C* **2014**, *118*, 10824–10832.
- 15 T. Morimoto, H. Nagao, *Bull. Chem. Soc. Jpn.* **1973**, *46*, 2000–2003.
- 16 R. Maskiewicz, D. Sogah, T. C. Bruice, *J. Am. Chem. Soc.* **1979**, *101*, 1347–1354.
- 17 J. Oguma, Y. Kakuma, S. Murayama, Y. Nosaka, *Appl. Catal. B. Environ.* **2013**, *129*, 282–286.
- 18 T. Hirakawa, Y. Nosaka, *J. Phys. Chem. C* **2008**, *112*, 15818–15823.
- 19 J. Zhang, Y. Nosaka, *J. Phys. Chem. C* **2013**, *117*, 1383–1391.
- 20 J. Zhang, Y. Nosaka, *Appl. Catal. B: Environ.* **2015**, *166–167*, 32–36.
- 21 B. H. J. Bielski, D. E. Cabelli, R. L. Arudi, A. B. Ross, *J. Phys. Chem. Ref. Data*, **1988**, *17*, 513–886.
- 22 T. Hirakawa, K. Yawata, Y. Nosaka, *Appl. Catal. A Gen.* **2007**, *325*, 105–111.
- 23 *Standard Potentials in Aqueous Solution*; (Eds.: A. J. Bard, R. Parsons, J. Jordan), Marcel Dekker: New York, **1985**.
- 24 Y. Nakabayashi, Y. Nosaka, *J. Phys. Chem. C* **2013**, *117*, 23832–23839.
- 25 O. I. Micic, Y. Zhang, K. R. Cromack, A. D. Trifunac, M. C. Thurnauer, *J. Phys. Chem.* **1993**, *97*, 1211–1283.
- 26 R. Nakamura, Y. Nakato, *J. Am. Chem. Soc.* **2004**, *126*, 1290–1298.
- 27 T. Ohno, K. Sarukawa, M. Matsumura, *New. J. Chem.* **2002**, *26*, 1167–1170.
- 28 J. Oguma, Y. Kakuma, M. Nishikawa, Y. Nosaka, *Catal. Lett.* **2012**, *142*, 1474–1481.
- 29 M. Nishikawa, R. Takanami, F. Nakagoshi, H. Suizu, H. Nagai, Y. Nosaka, *Appl. Catal. B. Environ.* **2014**, *160–161*, 722–729.

## ARTICLE

Journal Name

- 30 M. Minella, M. G. Faga, V. Maurino, C. Minero, E. Pelizzetti, S. Coluccia, G. Martra, *Langmuir* **2010**, *26*, 2521-2527.
- 31 P. A. Connor, K. D. Dobson, A. J. McQuillan, *Langmuir* **1999**, *15*, 2402-2408.
- 32 Z.-W. Qu, G.-J. Kroes, *J. Phys. Chem. B* **2006**, *110*, 8998-9007.
- 33 D. M. Savory, A. J. McQuillan, *J. Phys. Chem. C* **2013**, *117*, 23645-23656.
- 34 Y. Nosaka, M. Nakamura, T. Hirakawa, *Phys. Chem. Chem. Phys.* **2002**, *4*, 1088-1092.
- 35 A. Imanishi, K. Fukui, *J. Phys. Chem. Lett.* **2014**, *5*, 2108-2117.